Published in final edited form as:
BJU Int. 2013 August ; 112(4): . doi:10.1111/bju.12126.

Magnetic resonance imaging (MRI)-guided transurethral ultrasound therapy of the prostate: a preclinical study with radiological and pathological correlation using customised MRI-based moulds

Ari Partanen[1,2], **Nitin K. Yerram**[3], **Hari Trivedi**[3], **Matthew R. Dreher**[4], **Juha Oila**[5], **Anthony N. Hoang**[3], **Dmitry Volkin**[3], **Jeffrey Nix**[3], **Baris Turkbey**[6], **Marcelino Bernardo**[6,7], **Diana C. Haines**[8], **Compton J. Benjamin**[3], **W. Marston Linehan**[3], **Peter Choyke**[6], **Bradford J. Wood**[4], **Gösta J. Ehnholm**[5], **Aradhana M. Venkatesan**[4], and **Peter A. Pinto**[3,4]

[1]Philips Healthcare, Cleveland, OH, USA [2]Department of Physics, University of Helsinki, Helsinki, Finland [3]Urologic Oncology Branch, National Cancer Institute (NCI), National Institutes of Health (NIH), Bethesda, MD, USA [4]Center for Interventional Oncology, Radiology and Imaging Sciences, NIH Clinical Center and NCI, Bethesda, MD, USA [5]Philips Healthcare, Vantaa, Finland [6]Molecular Imaging Program, NCI, NIH, Bethesda, MD, USA [7]SAIC-Frederick, Inc., NCI-Frederick, Frederick, MD, USA [8]Pathology/Histotechnology Laboratory, Frederick National Laboratory for Cancer Research, NCI, Frederick, MD, USA

Abstract

- To characterise the feasibility and safety of a novel transurethral ultrasound (US)-therapy device combined with real-time multi-plane magnetic resonance imaging (MRI)-based temperature monitoring and temperature feedback control, to enable spatiotemporally precise regional ablation of simulated prostate gland lesions in a preclinical canine model.
- To correlate ablation volumes measured with intra-procedural cumulative thermal damage estimates, post-procedural MRI, and histopathology.
- Three dogs were treated with three targeted ablations each, using a prototype MRI-guided transurethral US-therapy system (Philips Healthcare, Vantaa, Finland).
- MRI provided images for treatment planning, guidance, real-time multi-planar thermometry, as well as post-treatment evaluation of efficacy.
- After treatment, specimens underwent histopathological analysis to determine the extent of necrosis and cell viability.
- Statistical analyses (Pearson's correlation, Student's *t*-test) were used to evaluate the correlation between ablation volumes measured with intra-procedural cumulative thermal damage estimates, post-procedural MRI, and histopathology.
- MRI combined with a transurethral US-therapy device enabled multi-planar temperature monitoring at the target as well as in surrounding tissues, allowing for safe, targeted, and controlled ablations of prescribed lesions.

Correspondence: Peter A. Pinto, Urologic Oncology Branch, National Cancer Institute, 10 Center Drive MSC 1210, Building 10, CRC, Room 2W-5940, Bethesda, MA 20892-1210, USA. pintop@mail.nih.gov.

- Ablated volumes measured by cumulative thermal dose positively correlated with volumes determined by histopathological analysis (r^2 0.83, $P < 0.001$).
- Post-procedural contrast-enhanced and diffusion-weighted MRI showed a positive correlation with non-viable areas on histopathological analysis (r^2 0.89, $P < 0.001$, and $r^2$0.91, $P = 0.003$, respectively).
- Additionally, there was a positive correlation between ablated volumes according to cumulative thermal dose and volumes identified on post-procedural contrast-enhanced MRI (r^2 0.77, $P < 0.01$).
- There was no difference in mean ablation volumes assessed with the various analysis methods ($P > 0.05$, Student's *t*-test).
- MRI-guided transurethral US therapy enabled safe and targeted ablations of prescribed lesions in a preclinical canine prostate model.
- Ablation volumes were reliably predicted by intra- and post-procedural imaging.
- Clinical studies are needed to confirm the feasibility, safety, oncological control, and functional outcomes of this therapy in patients in whom focal therapy is indicated.

Keywords

thermal ablation; therapeutic ultrasound; thermotherapy; minimally invasive therapy; magnetic resonance imaging; image-guided therapy

Introduction

Prostate cancer remains a leading medical problem in the USA. The introduction of PSA screening and earlier diagnosis of prostate cancer has shifted the treatment paradigm toward more localised therapy. In fact, up to 75% of patients are found to have localised disease [1]. Current whole-gland therapy offers the highest oncological efficacy in exchange for significant morbidities, which has motivated a growing interest in focal or regional treatment strategies that can achieve comparable oncological efficacy with minimal adverse effects on sexual and urinary function [2, 3]. Multiple phase I focal therapy trials, predominantly using cryotherapy, have shown the feasibility, safety, short-term oncological control, and minimal adverse effects profile [3]. Similar results were achieved in preliminary trials using laser-induced focal thermoablation of prostate cancer [3].

High temperatures (≥ 55 °C) are known to cause cytotoxic effects; a phenomenon defined as thermoablation [3-7]. Therapeutic ultrasound (US) is an emerging treatment method capable of achieving thermoablation in the prostate. US therapy may be used with either US or MRI guidance. Limitations of US include imprecise temperature monitoring, low sensitivity on cancer detection, and lack of three-dimensional (3D) imaging information. On the other hand, MRI can be used for monitoring real-time temperature changes in multiple planes, as well as for multi-parametric cancer detection, treatment planning, and for prediction of the extent of cell death using such sequences as contrast-enhanced imaging (CEI) and diffusion-weighted imaging (DWI).

Coupling therapeutic US with MRI guidance may be particularly efficacious for focal, regional, or whole-gland therapy of prostate cancer [7]. Preliminary clinical trials using transrectal high-intensity focused US (HIFU) for focal ablation of prostate cancer have reported fewer adverse events than traditional whole-gland therapy, suggesting that targeted focal or regional therapy may be safer [5, 8]. Despite these advances, transrectal HIFU has been complicated by long treatment times, incomplete cancer treatment (especially for

anterior lesions), erectile dysfunction, urinary incontinence, urethral stricture, and even recto-urethral fistulae. In comparison, transurethral US therapy has the potential to provide an even greater safety profile, while enabling targeted focal, regional, or whole-gland therapy of prostate cancer. Chopra *et al.* [9] and Siddiqui *et al.* [10] have successfully demonstrated regional prostate ablations in the clinic using a transurethral device.

The objective of the present study was to evaluate the feasibility and safety of a novel transurethral US-therapy device combined with real-time multi-plane MRI-based temperature monitoring and temperature feedback control to enable spatiotemporally precise regional ablation of simulated prostate gland lesions in a preclinical canine model. Moreover, we report on ablation spatiotemporal accuracy and correlate ablation volumes measured with intra-procedural cumulative thermal damage estimates, post-procedural MRI, and histopathology.

Materials and methods

In vivo experiment setup

Approved by the National Institutes of Health (NIH) Animal Care and Use Committee and in concordance with relevant guidelines, three non-castrated dogs (35–45 kg), having prostate volumes comparable with adult human male prostates, were included in this study. On the procedure day, the dogs received a warm water and mineral oil enema 2 h before US therapy, and were subsequently sedated using i.m. acepromazine (10 mg/mL) and hydromorphone (2 mg/mL) followed by cephalic i.v. catheterisation. Next, the dogs were induced with Propofol (10 mg/kg), intubated, and maintained under anaesthesia via continuous inhalation of isoflurane (2–4%). A 6-F Foley catheter was placed to empty the bladder until treatment. Each dog was continuously monitored by an experienced veterinary team throughout the procedure. A perineal urethrostomy was mandated in the dogs given the extreme curvature of the canine penile urethra in order to accommodate the US applicator, which was manually advanced to the level of the prostate. After treatment, the dogs were humanely killed using i.v. injection of sodium pentobarbital (150 mg/kg), followed by prostatic tissue procurement. To assess thermal damage to pelvic tissue, sections of muscle, rectum, and fat around the prostate were also resected during procurement and sent for histological analysis.

MRI-guided US-therapy system

A prototype MRI-guided US-therapy system (Philips Healthcare, Vantaa, Finland) with temperature feedback was used for administration of the US exposures (sonications). The system is similar to the one previously used by Chopra *et al.* [9], and includes a therapy control workstation using clinical software, a radiofrequency generator, a rigid, water-cooled transurethral US applicator (5 mm [15 F] diameter) with eight transducer elements (4 ×5 mm/element), a motor unit enabling rotation of the applicator, and a standard clinical MRI scanner (Achieva 3.0T, Philips Healthcare, Best, the Netherlands). For imaging, a standard MRI receiver coil was used for treatment planning, temperature mapping, and post-treatment imaging (32-channel SENSE Cardiac coil, Philips Healthcare, Best, the Netherlands). The coil was immobilised and consisted of 16 elements below the dog and 16 elements above (Fig. 1).

Sonications were done in continuous wave mode at 6.0 MHz. The applicator rotates about its long axis, with US beams propagating into the target tissue through a thin (25 μm) cylindrical polyester membrane. Acoustic coupling was achieved using US gel. Cooling of the anatomical near field (in this case the urethra) was achieved by means of a closed loop circuit of flowing room temperature degassed water between the transducer elements and

membrane. Ablation volume depth from the urethra and total size were controlled by adjusting the output power, sonication duration, and number of active transducer elements.

Treatment planning and MRI thermometry

MRI was used to plan sonications, monitor temperature changes during therapy, and to evaluate treatment outcome. Thermal dose (e.g. cumulative equivalent minutes at 43 °C [CEM_{43}]) is used to quantify thermal damage to tissue, and a dose of > 240 CEM_{43} can be used to indicate ablative exposures [11].

T_2-weighted turbo spin-echo (TSE) images used for treatment planning were acquired as 2D multi-slice stacks in coronal, sagittal, and axial planes. The prostate was clearly visible, as shown in Figs. 1 and 2.

Temperature elevations during US therapy were monitored using rapid multi-planar MRI thermometry. Seven axial slices and one sagittal slice were acquired with a spatial resolution of 1.5 × 1.5 × 5 mm^3 for each dynamic cycle resulting in a temporal update rate of 4.1 s/8 slices. The slices were positioned parallel to the US beams (Figs. 1 and 2), allowing for temperature monitoring and thermal dose calculations at the target as well as in surrounding tissues. Real-time temperature and thermal dose maps were calculated using the proton-resonance frequency shift (PRFS, 0.0094 ppm/ °C) technique [12] and displayed as 2D colour-coded overlays on top of the anatomical images (Fig. 2). Temperature maps were corrected for baseline drift by subtracting the average apparent temperature change of all voxels in a freehand-drawn reference region (axial slice) in nearby muscle, outside the heated region.

After US therapy, the axial T_2-weighted images were reacquired, followed by a T_1-weighted fast-field echo (T1-FFE) CEI sequence using clinically approved gadolinium-based contrast agent (Magnevist, 0.1 mmol/kg). In the second and third dogs treated, 2D multi-slice DWI was also performed before contrast agent injection. Previous studies have validated the use of both CEI and DWI to visualise necrotic tissue [13, 14]. Additional details and MRI-sequence parameters may be found in Appendix A.

Ablation feedback control

Before ablations, a test sonication (P_{ac} = 1.1 W/channel, 1–3 active elements, t = 10–20 s) was performed to confirm transducer angle, location of heating, and the quality of acoustic coupling. Between sonications, the transducer was rotated to the next position using control software, and a cool down period (> 10 min) was used to ensure return to baseline temperature. This heat and cool cycle was repeated three times (three discrete locations) in each canine prostate.

Point targets were intentionally selected in the prostatic central zone, transitional zone and peripheral zone, in order to assess the feasibility of ablation in these locations. Temperature feedback was used to control ablation in the target region. A single control point (5 voxels) provided temperature feedback at a user-defined radial distance from the applicator (1.0–1.8 cm, depending on the size of the prostate). The power level was kept constant for all independent sonications (range 1.1–1.8 W acoustic power/channel, Appendix B) and sonication was automatically stopped when the mean temperature in this control point reached 56 °C [15]. Parameters for all sonications are listed in Appendix B.

Treatment analysis

Sonication data analysis was performed in Matlab 7.0 (MathWorks, Natick, MA, USA) and in IDL 6.1 (ITT Visual Information Solutions, Boulder, CO, USA). The mean temperature at

the control point and the maximum temperature within the heated region of the prostate were analysed from the axial slices of MRI thermometry images. Furthermore, thermal dose (> 240 CEM_{43}) volumes were calculated according to the Sapareto-Dewey equation [16]. The temperature map mean noise level was calculated as time-averaged temperature standard deviation in an unheated region.

Non-perfused volumes and volumes of greater diffusion (indicative of thermal ablation) were measured from CEIs and DWIs, respectively, using OsiriX Imaging Software v.3.7 (Geneva, Switzerland).

Histopathological analysis

To obtain precise MRI–histopoathology correlation, a 3D printed plastic prostate mould unique for each dog was created using the post-treatment T_2-weighted images, as previously described [17-19]. After resection, prostates were fixed in 10% formalin for 24 h. Using the mould, the prostate was then sliced every 4.5 mm to achieve congruence with MRI axial slices (acquired with 1.5 mm spacing/thickness). Subsequently, specimens were placed in 10% formalin and sent for cytokeratin-8 (CK8) and haematoxylin and eosin (H&E) staining. Formalin-fixed prostate slices were photographed and routinely processed, paraffin-embedded, and sectioned at 5 μm. Step sections at 1.5-mm intervals were taken of slices showing grossly visible lesions. Alternating serial sections were stained with H&E or underwent immunohistochemistry for detection of CK8: after 30 min of 0.1% trypsin antigen retrieval and blocking with normal horse serum, ready-to-use CK8 antibody (CAM 5.2; BD Bioscience #349205) was applied for 40 min at room temperature. Secondary antibody (biotinylated horse anti-mouse IgG), followed by ABC Elite, 3,3'-diaminobenzidine, and haematoxylin counterstaining was performed. Stained sections were scanned into digital format via an Aperio Scanscope XT (Vista, CA, USA). Digital images were evaluated and annotated by a Board Certified veterinary pathologist (D.C.H.) using Aperio ImageScope software.

On histology, cell viability was measured using vital stain CK8 (CAM 5.2) [20,21]. Areas of non-viable cells were marked with absence of stain. Histological ablation volumes were calculated using the cross-sectional non-viable area of each ablation and the known slice thickness of individual specimens. While shrinkage of formalin-fixed specimens has been reported [22], uncorrected volumes are reported in this study.

Statistical analysis

Pearson's correlation coefficients were calculated to evaluate the correlation between ablation volumes as determined by thermal dose, CEI, DWI, and histology. The Student's *t*-test was used to determine differences in ablation volumes with the various analysis methods. Values are reported as the mean (SD). A $P < 0.05$ was considered to indicate statistical significance.

Results

MRI

MRI was used for treatment planning and temperature monitoring (Fig. 2). Initial planning images enabled identification of the prostate and prescription of sonication locations (Fig. 2 A and B). Temperature elevations (Fig. 2 C and D) corresponded within 1 ° of the targeted sonication angle, as well as with the width and length of the active transducer elements. Temperature maps had a mean (SD) noise level of 0.3 (0.1) °C.

Ablation feedback control

In all, nine sonications were performed in three dogs. Early in the study, one sonication was manually stopped at 180 s due to selection of a power inadequate to sufficiently elevate the prostate temperature. All other sonications were stopped automatically after control point target temperature (56 °C) was reached. Sonication results are summarised in Appendix B.

Sonications resulted in temperature elevations with the major axis in the direction of the US beam propagation (Fig. 2 C and D). The mean temperature within the control point, and maximum temperature within the heated region ($\Delta T > 2$ °C) over a 124-s sonication are shown in Fig. 3. For all feedback-controlled sonications, the mean time required to achieve target temperature (56 °C) at the control point was 66–186 s (depending on control point distance, applied power, and local tissue characteristics), at which point the temperature feedback algorithm appropriately stopped the sonication. Upon sonication completion, temperature returned to baseline levels after 3–5 min. Agreement of temperature before and after sonication suggests that the magnetic drift correction was correctly applied in order to obtain accurate thermal maps (Fig. 3).

Thermal dose estimation, image analysis, and histopathological analysis

Representative examples of CEI, DWI, CK8-stained tissue, and thermal dose estimates are shown in Fig. 4. CEIs were obtained in each dog after completion of treatment (Fig. 4A) for visualisation of non-perfused volume. The mean (SD, range) non-perfused volume per sonication was 0.49 (0.30, 0.13–0.96) cm^3 (Table 1). DWIs, obtained in the last two dogs after treatment (Fig. 4B), showed a mean (SD, range) ablated volume of per sonication 0.54 (0.29, 0.19–0.87) cm^3 (Table 1). The mean (SD, range) non-viable tissue volume on histopathological analysis (CK8, Fig. 4C) per sonication was 0.55 (0.29, 0.14–0.96) cm^3 (Table 1). Real-time assessment of thermal dose provided ablation volume estimates during treatment, as shown in Fig. 4D. According to a thermal dose threshold of 240 CEM_{43}, the mean (SD, range) ablated volume per sonication was 0.84 (0.43, 0.1–1.42) cm^3 (Table 1). In all specimens, regions of thermocoagulation were detected and noted to be within the prostate capsule, with no thermal damage to the peri-prostatic tissues.

Volume correlation analysis

There was a positive correlation between ablated volume using cumulative thermal dose and histopathological analysis (r^2 0.83, $P < 0.001$, Fig. 5A), and between cumulative thermal dose and post-procedural CEI (r^2 0.77, $P < 0.01$, Fig. 5D). Similarly, CEI and DWI showed a positive correlation with histopathological analysis (r^2 0.89, $P < 0.001$, Fig. 5B; and r^2 0.91, $P < 0.01$, Fig. 5C, respectively). There were no differences in means for the ablated volumes in any of the above analysis methods ($P > 0.05$, Student's *t*-test).

Discussion

Minimally invasive prostate cancer therapy represents an evolving paradigm shift that may achieve reliable oncological efficacy with minimal morbidity. Emerging novel focal or regional ablative therapies include laser ablation, cryotherapy, and US [3]. The use of ablative hyperthermia for treatment of prostate cancer may be efficacious [3], and many trials have shown the value of transrectal HIFU in cancer control [5, 8, 23, 24]. However, transrectal HIFU is still plagued with significant morbidities [7] and long treatment times.

Transurethral US therapy has considerable potential predicted by prior successes using transrectal HIFU as focal treatment [3,5, 8]. While it is estimated that up to 80% of prostate cancer is multifocal in nature, the remaining 20% could be potential focal therapy candidates for a curative intent. Additionally, it is thought that not all lesions are equivalent in terms of

their propensity to grow and metastasize. Although controversial, the existence of a dominant index lesion responsible for cancer progression and metastasis has been proposed by many experts [25]. Given recent controversies about potential overtreatment of clinically insignificant disease, targeted treatment of an index lesion may be a viable and practical solution [3, 25]. In this case, focal and/or regional treatment may be effective as a cancer control method.

Limitations of TRUS imaging and TRUS biopsy have been well documented. Multi-parametric MRI has been shown to be better than TRUS biopsy in the detection of prostate cancer [26]. Furthermore, some studies have reported cancer detection specificity and sensitivity as high as 0.94 and 0.84 for T_2-weighted MRI alone, significantly improving when multiple parameters are combined [27]. Coupling multi-parametric MRI with a transurethral US-therapy device may allow for accurate diagnosis, targeting, and treatment of cancer foci.

Our preliminary results suggest that MRI-guided transurethral US therapy is safe and feasible, allowing for both spatially accurate and precise treatment of prostate cancer. Using real-time multi-planar and multi-slice temperature monitoring with automated temperature feedback control, it is possible to reach ablative temperatures in targeted regions, while avoiding excess temperature elevation in critical anatomical areas. Thermal damage to the urethra may be avoided by flowing degassed water between the transducer elements and the membrane, cooling the anatomical near field during sonications. In the present study, target locations were located in the central zone, transitional zone, and peripheral zone, showing adequate sonication depth in treatment of all lesions in the prostate (Fig. 4). It is critical to achieve effective, targeted treatment of peripheral prostate cancer lesions while avoiding extra-prostatic thermal damage, given that most prostate cancers reside in the peripheral zone and the proximity of these tumours to the neurovascular bundles. Maintaining the integrity of vulnerable regional anatomy while achieving oncological efficacy will be one of the main objectives when translating transurethral MRI-guided US therapy to clinical care.

MRI provided a high-resolution imaging method for real-time anatomical and temperature monitoring. Some bias (slope = 0.59–0.89) was seen when correlating histological analysis (i.e. gold standard) to MRI, although ablation volume estimates, using thermal dose, CEI, and DWI significantly correlated with histology (r^2 0.77–0.91, all $P < 0.05$). Possible causes of this bias include tissue shrinkage during fixation and a change in reference temperature during treatment. Because thermal dose calculations rely on a relative change from a reference temperature that is obtained immediately before sonication, a drop in core body temperature over the course of treatment could considerably influence the thermal dose estimates. In future experiments, core body temperature should be serially monitored to eliminate this error. In addition, active cooling of urethra may have created a temperature gradient within the prostate, which was not accounted for in the thermal dose estimates.

Further limitations in the present study include performing only one ablation in each target region, which fails to fully simulate a clinical procedure, in which multiple ablations (or a continuous ablation using rotational control) are targeted upon a single cancerous region creating a tumour-free treatment margin. Moreover, the short- or long-term outcomes of transurethral US ablations were not assessed in the present study. However, Siddiqui *et al.* [10] have previously reported on the use of transurethral US for whole-gland therapy, showing that there were no major, negative side-effects in the dogs 48 h after surgery.

Whereas these results are encouraging, further experiments are needed to optimise transurethral MRI-guided US therapy for use in humans. In these initial experiments, the transducer was rigid and remained stationary during sonications. However, as the applicator

can be rotated and the transducer elements can be individually activated and power modulated, the system does have the flexibility to perform either regional or whole-gland ablations, allowing precise control of ablation [9, 28]. Future experiments can take advantage of particularly the rotational control: rotating the transducer while sonicating may allow for larger ablation volumes in a shorter period, as validated by other groups [9, 10]. Moreover, a flexible US applicator could facilitate urethral placement similarly to a Foley urethral catheter. This thermoablative therapy could potentially be applied to the treatment of BPH. The potential and flexibility of this transurethral device to rapidly provide focal, regional, or whole-gland therapy is attractive in comparison with other prostate cancer-therapy devices.

In conclusion, coupling MRI with a transurethral US-therapy device enabled multi-planar temperature monitoring at the target as well as in surrounding tissues, allowing for safe, targeted, and controlled ablations of prescribed prostatic lesions in a canine model. Non-viable tissue volumes at histopathological analysis correlated well with thermal dose estimates and ablation volumes seen on MRI. These preliminary data underscore the value of future clinical studies to confirm the feasibility, safety, oncological control, and functional outcomes of this treatment for prostate cancer.

Acknowledgments

The authors thank Dr Max Köhler for his advice, and acknowledge support from SalWeOy/TEKES. In addition, the authors thank Dr Rajiv Chopra for his guidance and advice.

This research was supported (in part) by the Center for Interventional Oncology and Intramural Research Program of the NIH, and through a Cooperative Research and Development Agreement (CRADA) with Philips Healthcare. Ari Partanen, Juha Oila, and Dr Gösta Ehnholm are paid employees of Philips Healthcare. The content of this publication does not necessarily reflect the views or policies of the Department of Health and Human Services, nor does mention of trade names, commercial products, or organizations imply endorsement by the USA Government.

References

1. Cooperberg MR, Broering JM, Litwin MS, et al. The contemporary management of prostate cancer in the United States: lessons from the cancer of the prostate strategic urologic research endeavor (CapSURE), a national disease registry. J Urol. 2004; 171:1393–401. [PubMed: 15017184]
2. Hoang AN, Volkin D, Yerram NK, et al. Image guidance in the focal treatment of prostate cancer. Curr Opin Urol. 2012; 22:328–35. [PubMed: 22647649]
3. Lindner U, Trachtenberg J, Lawrentschuk N. Focal therapy in prostate cancer: modalities, findings and future considerations. Nat Rev Urol. 2010; 7:562–71. [PubMed: 20842187]
4. Hildebrandt B, Wust P, Ahlers O, et al. The cellular and molecular basis of hyperthermia. Crit Rev Oncol Hematol. 2002; 43:33–56. [PubMed: 12098606]
5. Ahmed HU, Freeman A, Kirkham A, et al. Focal therapy for localized prostate cancer: a phase I/II trial. J Urol. 2011; 185:1246–54. [PubMed: 21334018]
6. Lindner U, Lawrentschuk N, Weersink RA, et al. Focal laser ablation for prostate cancer followed by radical prostatectomy: validation of focal therapy and imaging accuracy. Eur Urol. 2010; 57:1111–4. [PubMed: 20346578]
7. Lukka H, Waldron T, Chin J, et al. High-intensity focused ultrasound for prostate cancer: a systematic review. Clin Oncol (R Coll Radiol). 2011; 23:117–27. [PubMed: 20932728]
8. Ahmed HU, Hindley RG, Dickinson L, et al. Focal therapy for localised unifocal and multifocal prostate cancer: a prospective development study. Lancet Oncol. 2012; 13:622–32. [PubMed: 22512844]
9. Chopra R, Colquhoun A, Burtnyk M, et al. MR Imaging-controlled Transurethral Ultrasound Therapy for Conformal Treatment of Prostate Tissue: Initial Feasibility in Humans. Radiology. 2012; 265:303–13. [PubMed: 22929332]

10. Siddiqui K, Chopra R, Vedula S, et al. MRI-guided transurethral ultrasound therapy of the prostate gland using real-time thermal mapping: initial studies. Urology. 2010; 76:1506–11. [PubMed: 20709381]
11. Meshorer A, Prionas SD, Fajardo LF, Meyer JL, Hahn GM, Martinez AA. The effects of hyperthermia on normal mesenchymal tissues. Application of a histologic grading system. Arch Pathol Lab Med. 1983; 107:328–34. [PubMed: 6687797]
12. Ishihara Y, Calderon A, Watanabe H, Okamoto K, Suzuki Y, Kuroda K. A precise and fast temperature mapping using water proton chemical shift. Magn Reson Med. 1995; 34:814–23. [PubMed: 8598808]
13. Chen J, Daniel BL, Diederich CJ, et al. Monitoring prostate thermal therapy with diffusion-weighted MRI. Magn Reson Med. 2008; 59:1365–72. [PubMed: 18506801]
14. Jacobs MA, Herskovits EH, Kim HS. Uterine fibroids: diffusion-weighted MR imaging for monitoring therapy with focused ultrasound surgery--preliminary study. Radiology. 2005; 236:196–203. [PubMed: 15987974]
15. Chopra R, Tang K, Burtnyk M, et al. Analysis of the spatial and temporal accuracy of heating in the prostate gland using transurethral ultrasound therapy and active MR temperature feedback. Phys Med Biol. 2009; 54:2615–33. [PubMed: 19351975]
16. Sapareto SA, Dewey WC. Thermal dose determination in cancer therapy. Int J Radiat Oncol Biol Phys. 1984; 10:787–800. [PubMed: 6547421]
17. Trivedi H, Turkbey B, Rastinehad AR, et al. Use of patient-specific MRI-based prostate mold for validation of multiparametric MRI in localization of prostate cancer. Urology. 2012; 79:233–9. [PubMed: 22202553]
18. Shah V, Pohida T, Turkbey B, et al. A method for correlating in vivo prostate magnetic resonance imaging and histopathology using individualized magnetic resonance-based molds. Rev Sci Instrum. 2009; 80:104301. [PubMed: 19895076]
19. Turkbey B, Mani H, Shah V, et al. Multiparametric 3T prostate magnetic resonance imaging to detect cancer: histopathological correlation using prostatectomy specimens processed in customized magnetic resonance imaging based molds. J Urol. 2011; 186:1818–24. [PubMed: 21944089]
20. Makin CA, Bobrow LG, Bodmer WF. Monoclonal antibody to cytokeratin for use in routine histopathology. J Clin Pathol. 1984; 37:975–83. [PubMed: 6206100]
21. Van Leenders GJ, Beerlage HP, Ruijter ET, de la Rosette JJ, van de Kaa CA. Histopathological changes associated with high intensity focused ultrasound (HIFU) treatment for localised adenocarcinoma of the prostate. J Clin Pathol. 2000; 53:391–4. [PubMed: 10889823]
22. Jonmarker S, Valdman A, Lindberg A, Hellstrom M, Egevad L. Tissue shrinkage after fixation with formalin injection of prostatectomy specimens. Virchows Arch. 2006; 449:297–301. [PubMed: 16909262]
23. Foster RS, Bihrle R, Sanghvi N, et al. Production of prostatic lesions in canines using transrectally administered high-intensity focused ultrasound. Eur Urol. 1993; 23:330–6. [PubMed: 7683997]
24. Gelet A, Chapelon JY, Margonari J, et al. Prostatic tissue destruction by high-intensity focused ultrasound: experimentation on canine prostate. J Endourol. 1993; 7:249–53. [PubMed: 8358423]
25. Ahmed HU. The index lesion and the origin of prostate cancer. N Engl J Med. 2009; 361:1704–6. [PubMed: 19846858]
26. Sciarra A, Barentsz J, Bjartell A, et al. Advances in magnetic resonance imaging: how they are changing the management of prostate cancer. Eur Urol. 2011; 59:962–77. [PubMed: 21367519]
27. Turkbey B, Pinto PA, Mani H, et al. Prostate cancer: value of multiparametric MR imaging at 3 T for detection – histopathologic correlation. Radiology. 2010; 255:89–99. [PubMed: 20308447]
28. Diederich CJ, Stafford RJ, Nau WH, Burdette EC, Price RE, Hazle JD. Transurethral ultrasound applicators with directional heating patterns for prostate thermal therapy: in vivo evaluation using magnetic resonance thermometry. Med Phys. 2004; 31:405–13. [PubMed: 15000627]

Abbreviations

CEI	contrast-enhanced imaging/images
CEM_{43}	cumulative equivalent minutes at 43 °C
CK8	cytokeratin-8
((3)(2)D	(three) (two) dimensional
DWI	diffusion-weighted imaging/images
FFE	fast-field echo
H&E	haematoxylin and eosin
HIFU	high-intensity focused ultrasound
NIH	National Institutes of Health
PRFS	proton-resonance frequency shift
TSE	turbo spin-echo
US	ultrasound

What's known on the subject? and What does the study add?

Focal ablative therapy continues to be investigated as an alternative treatment option for organ-confined prostate cancer. Therapeutic ultrasound (US) is an emerging treatment method capable of achieving minimally invasive, precise, and conformal thermoablation in the prostate. Yet reports on the urological application of this technology have been scant. Under magnetic resonance imaging (MRI)-guidance, a transurethral US applicator has the potential to accurately and reliably ablate cancer foci or cancer-associated prostatic regions, while minimising the morbidities associated with conventional whole-gland resection or therapy.

The present study evaluates the feasibility and safety of a novel transurethral US-therapy device combined with real-time multi-plane MRI-based temperature monitoring and temperature feedback control. Moreover, we report on ablation spatiotemporal accuracy and correlate ablation volumes measured with MRI and histopathology.

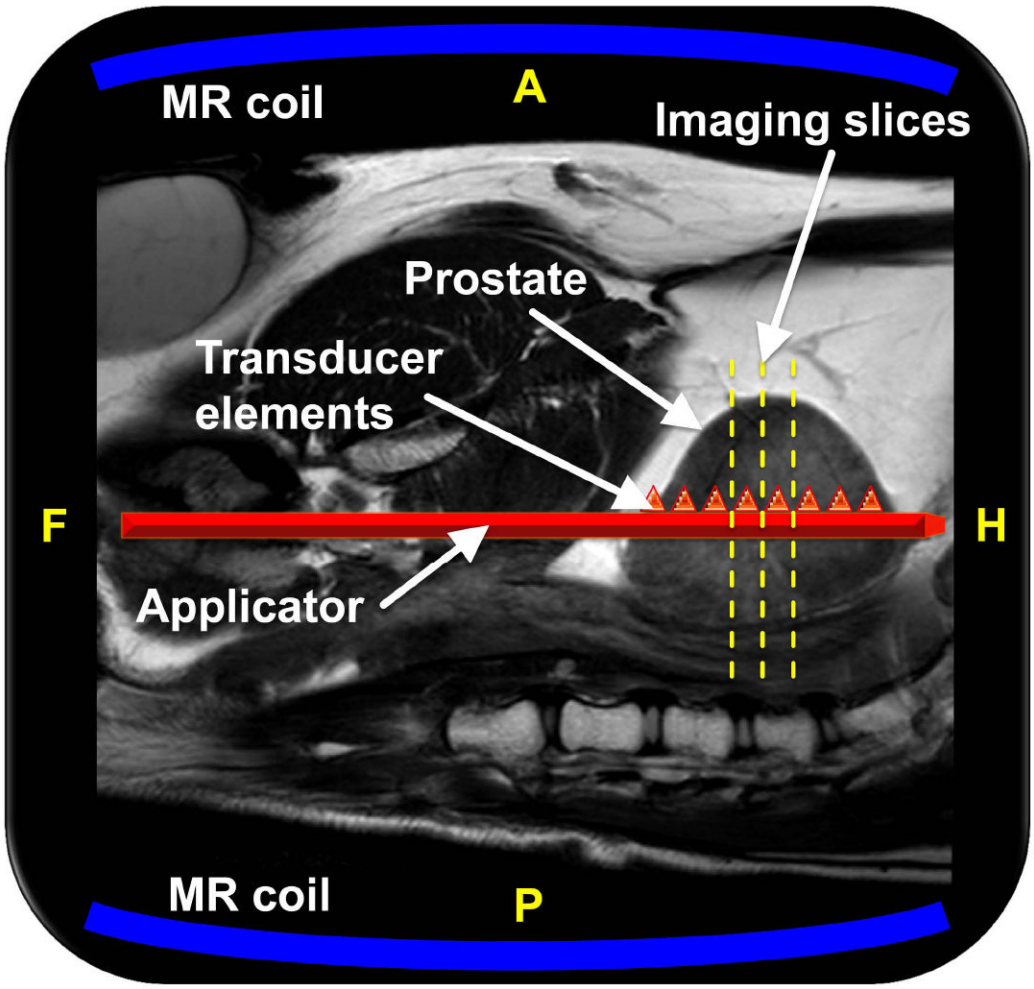

Figure 1.
Schematic of the MRI-guided US therapy setup. The sagittal imaging plane is shown, with the dog supine on the MRI table top, and the US applicator shown in red is advanced along the urethra to the level of the prostate. The central three axial imaging slice positions for the thermometry sequence are shown with yellow dashed lines, and the two MRI coils are depicted in blue. Depiction of the applicator and its eight transducer elements as triangles within the prostate are meant to be illustrative. A, P, F, and H denote anterior, posterior, feet, and head, respectively.

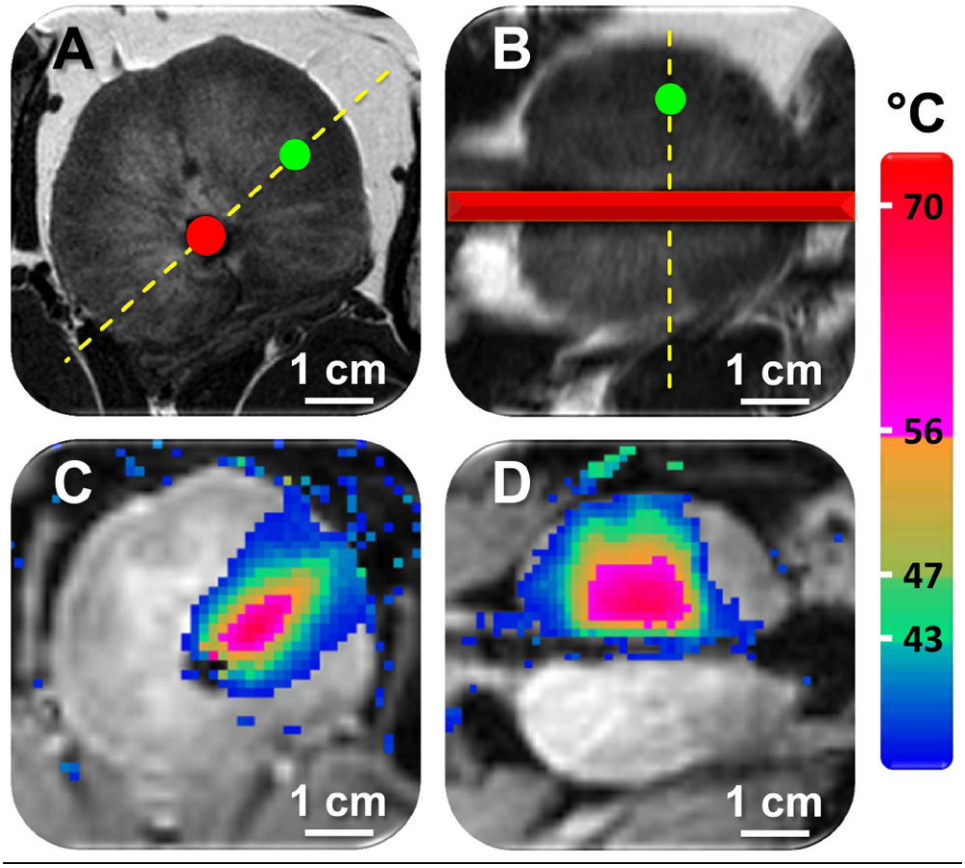

Figure 2.

Planning and temperature mapping for a focal prostate ablation using MRI-guided US therapy. A and B) Prostate was clearly identified on the T_2-weighted axial and sagittal planning images, and a temperature feedback control point within the prostate was prescribed (green circle). The red overlay shows the position of the US applicator, and the dashed yellow lines depict the position of the imaging slices (A shows the slice position in B, and B shows the slice position in A). Depiction of applicator within the prostate is meant to be illustrative. C and D) Colour-coded temperature maps overlaid on dynamic magnitude images during a sonication (using four transducer elements), showing typical temperature distribution at the end of a 124 s sonication. Temperature monitoring and control was achieved in the target location with fast-field echo (FFE)-echo planar imaging (EPI) sequence, using the PRFS method for temperature mapping, and by using a binary temperature feedback algorithm. B and D are the sagittal image planes corresponding to A and C, respectively.

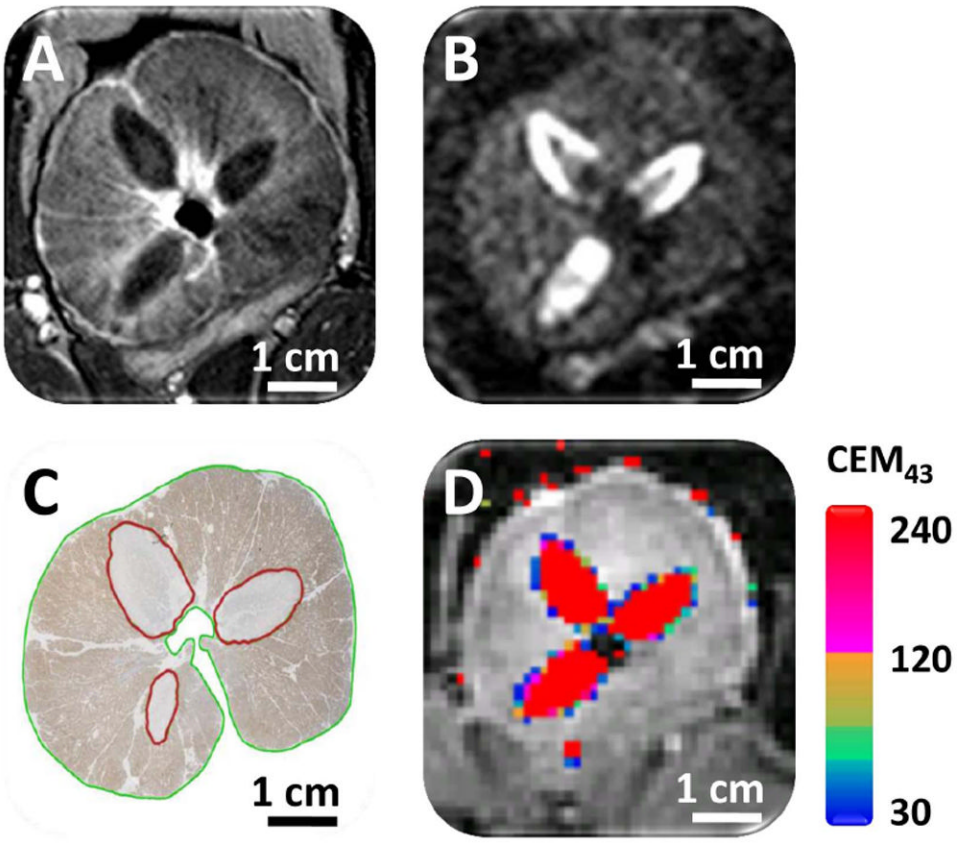

Figure 3.
Representative examples of mean (solid), standard deviation (dotted) and maximum (dashed) temperatures over a 124 s sonication, analysed from the axial slices. The maximum temperature curve shows the measured maximum temperature within the heated region, while the mean temperature curve depicts the mean temperature with standard deviations within the predefined control point (5 voxels). Sonication was automatically stopped when the control point mean temperature reached 56 °C.

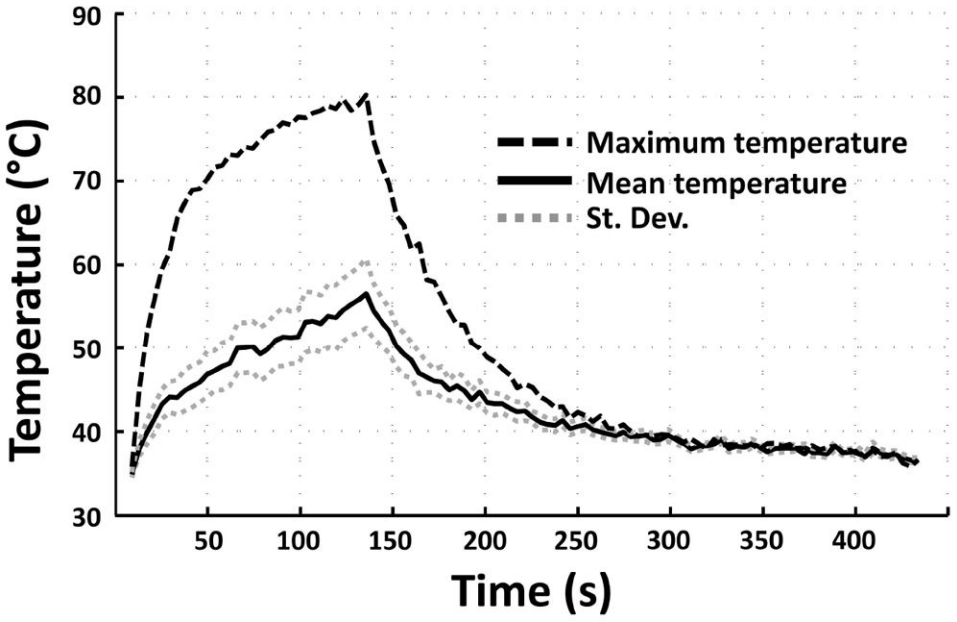

Figure 4.

Representative examples of A) CEI showing non-perfused regions, B) DWI (b-value = 2000) showing greater diffusion in ablated regions, C) CK8 stained tissue showing areas of non-viable tissue, and D) real-time cumulative thermal dose estimates. Ablated volumes on histology appear slightly distorted compared with MRI due to differences in tissue slice position and shrinkage secondary to formalin fixation.

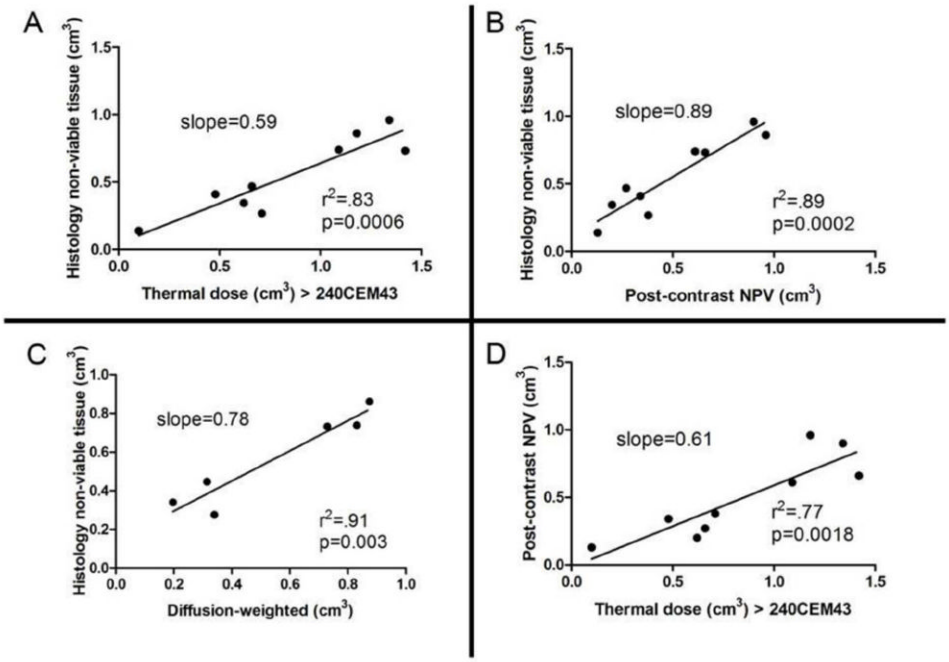

Figure 5.

Correlation of histology and MRI-ablation volume estimates for all independent sonications. A) Histologically non-viable tissue as a function of thermal dose, where CEM_{43} > 240 was used as the threshold for tissue necrosis. B) Histologically non-viable tissue as a function of non-perfused volumes on post-treatment CEI. C) Histologically non-viable tissue as a function of ablated volumes on DWI. D) Non-perfused volumes on post-treatment CEI as a function of thermal dose.

Table 1

Analysis results for cumulative thermal dose volumes, non-perfused tissue volumes, non-viable tissue volumes, and tissue volumes with greater diffusion, calculated from thermal dose maps, CEI, histopathology images, and DWI, respectively. DWI was only performed in dogs 2 and 3.

	Dog 1				**Dog 2**				**Dog 3**			
Total prostate volume, cm^3	**34.2**				**48.9**				**27.6**			
	Thermal dose	**CEI**	**Histol.**	**DWI**	**Thermal dose**	**CEI**	**Histol.**	**DWI**	**Thermal dose**	**CEI**	**Histol.**	**DWI**
Ablation 1	0.1	0.13	0.14	N/A	1.18	0.96	0.86	0.87	0.71	0.38	0.28	0.34
Ablation 2	0.48	0.34	0.41	N/A	1.42	0.66	0.73	0.72	0.66	0.27	0.45	0.31
Ablation 3	1.34	0.9	0.96	N/A	1.09	0.61	0.74	0.83	0.62	0.2	0.34	0.19

Appendix A

MRI parameters

Sequence purpose	MRI sequence	TR, ms	TE, ms	Flip angle	FOV, mm^2	Slice thickness, mm	NSA	Spatial resolution, mm	TSE/EPI factor	Seq. specific	Scantime, s
Planning	MS T_2wTSE (COR+SAG)	1613	60	90	140×140	3.0	2	0.46×0.58×3.0	12	-	132
Planning	MS T_2wTSE (TRA)	2227	60	90	120×120	1.5	2	0.4×0.4×1.5	11	-	245
Thermometry	MS FFE-EPI	34	16	20	160×160	5.0	1	1.5×1.5×5	9	SPIR fat suppr.	4.1 (/dyn.)
DWI	MS DWI-EPI	3896	60	90	140×140	2.73 (gap 0.3)	6	1.25×1.29×2.73	1	b-factor 2000	74
SEI	3D FFE CE (PRE+POST)	10	2.9	20	120×120	1.5	10	1.48×1.48×1.5	-		494

COR, coronal; SAG, sagittal; TRA, transverse; EPI, echo planar imaging;TR, repetition time; TE, echo time; FOV, field of view; NSA, number of signal averages.

Appendix B

Sonication parameters, durations, and resulting temperatures for all sonications. The control point distance denotes the distance from the transducer to the location used for temperature feedback control.

	Dog 1			Dog 2			Dog 3		
	Sonic. 1 (*)	**Sonic. 2**	**Sonic. 3**	**Sonic. 1**	**Sonic. 2**	**Sonic. 3**	**Sonic. 1**	**Sonic. 2**	**Sonic. 3**
Elements in use, n	4	4	4	4	4	4	3	3	3
Total acoustic power, W	4.32	5.76	5.76	5.76	7.2	5.76	4.32	4.32	4.32
Control point distance, mm	12	14	12	14	18	14	12	12	10
Sonication duration, s	180	172	147	99	124	186	66	145	65
Mean T (°C) in control point	48.04	56.46	56.53	56.19	56.54	56.29	56.87	56.86	56.69
Max. T (°C) in heated region	55.23	83.63	72.41	74	80.27	73.94	77.49	71.3	68.37

* The mean temperature at the end of sonication was calculated from 5 voxels at the control point. All sonications were performed at a frequency of 6.0 MHz. Sonication marked with an asterisk was manually stopped at 180 s due to a too low power setting (insufficient temperature elevation).